Supplementary Information to: The effect of uncertainties in natural forcing records on simulated temperature during the last Millennium

Lucie Lücke[1], Andrew P Schurer[1], Matthew Toohey[2], Lauren R Marshall[3, 4], and Gabriele C Hegerl[1]

[1]School of Geosciences, University of Edinburgh, Edinburgh, UK
[2]Institute of Space and Atmospheric Studies, University of Saskatchewan, Saskatoon, SK, Canada
[3] Yusuf Hamied Department of Chemistry, University of Cambridge, Cambridge, UK
[4] Now at: Department of Earth Sciences, Durham University, Durham, UK

October 2022

1 Data and method

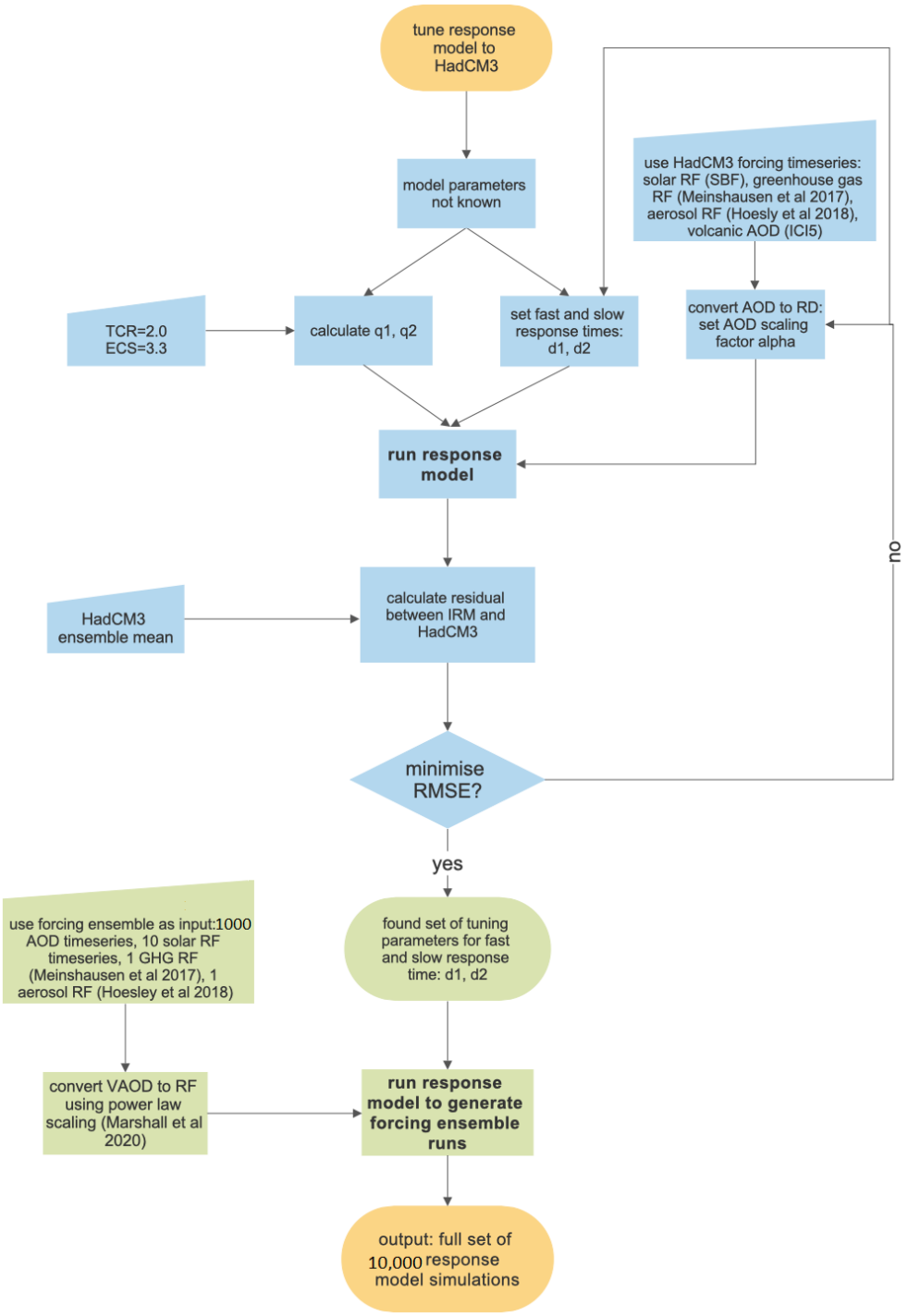

Figure S1: Flowchart of the tuning process (blue) followed by the generation of the forcing uncertainty ensemble simulations (green).

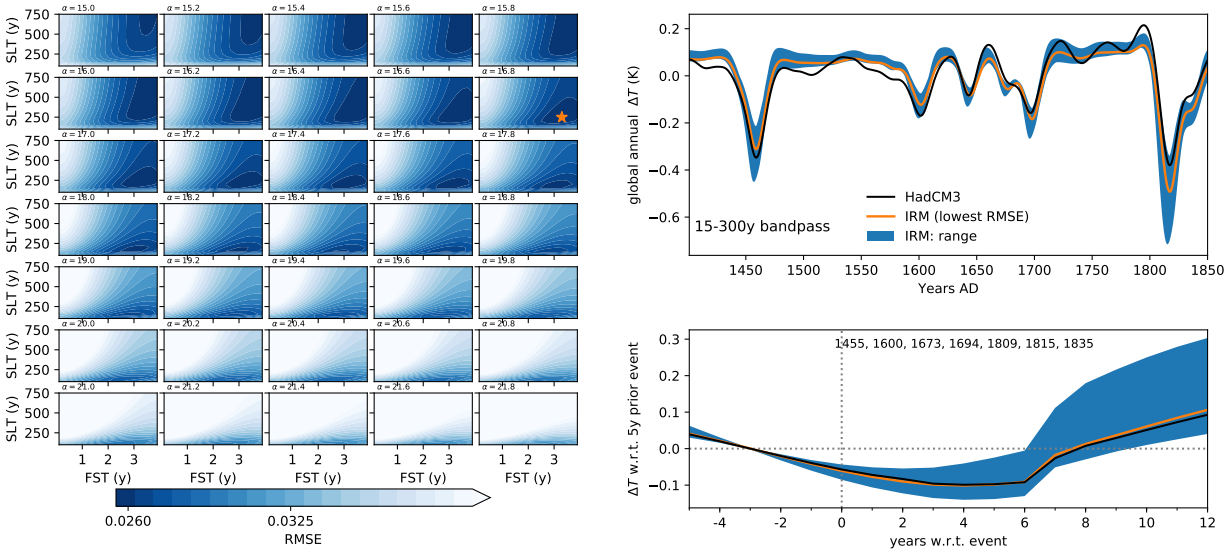

Figure S2: Left panels: RMSE for fast (FST) versus slow response time (SLT), each panel has a fixed AOD scaling α. The minimum RMSE is marked by a golden star on the corresponding panel. Top right: timeseries of the impulse response model (IRM) volcanic only run versus the mean of 8 HadCM3 volcanic only simulations. Bottom left: superposed epoch analysis for the seven largest eruptions in ICI5. Target: global annual land and ocean surface temperature, filtered by a 15-300y bandpass filter.

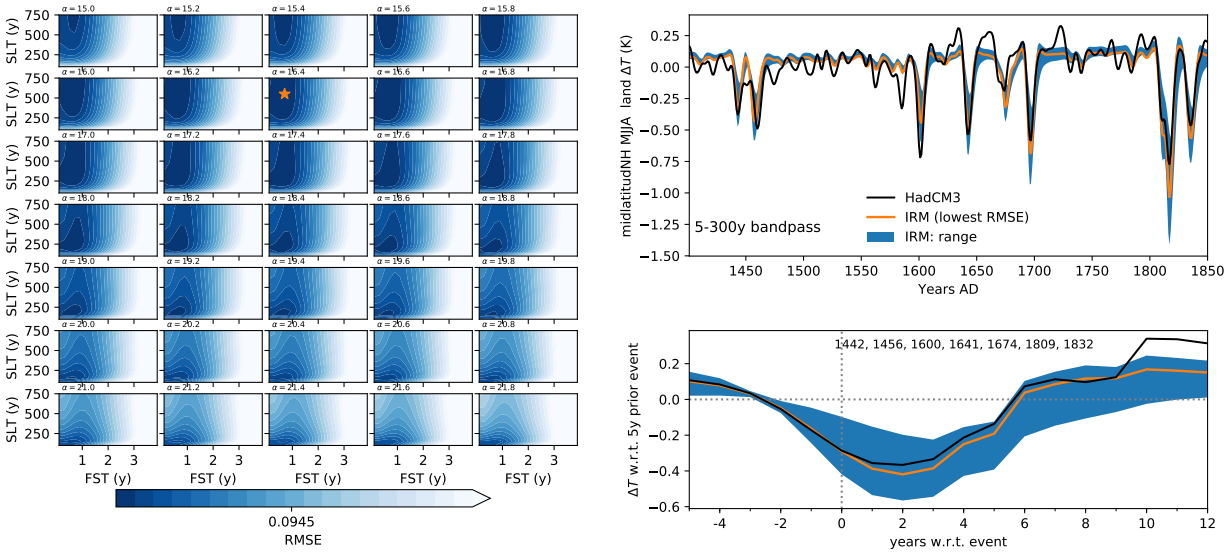

Figure S3: As previous but for tuning to midlatitudinal NH summer (MJJA).

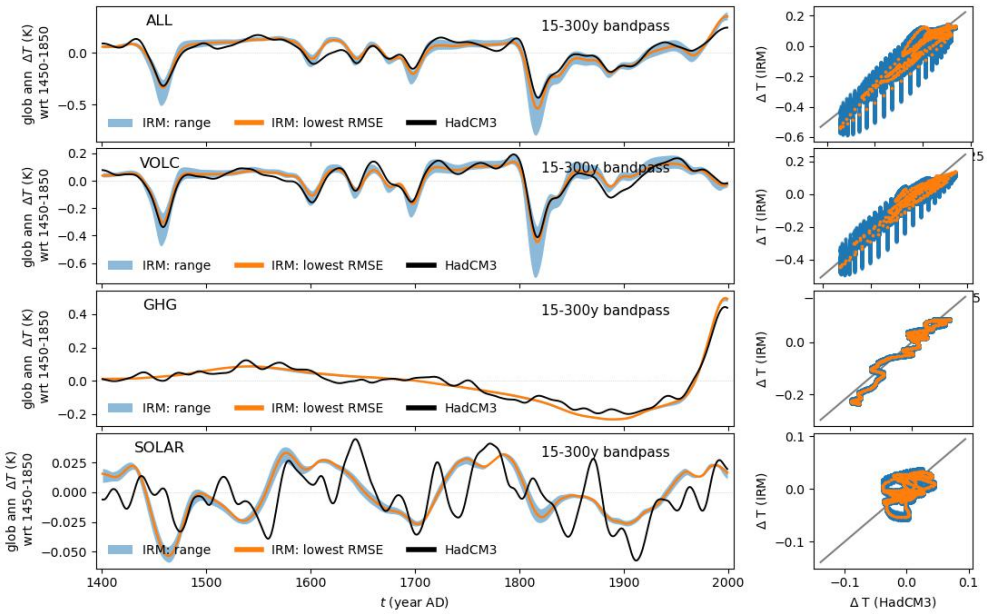

Figure S4: HadCM3 ensemble mean versus the response model output and the best fit during the tuning process. Left: Timeseries of the model runs, using (from top to bottom): all forcings, volcanic forcing only, greenhouse gas forcing only, solar forcing only. Right: scatter plot of the timeseries as shown on the left panel: HadCM3 ensemble mean versus each response model run. Colours as stated in legend on left panels.

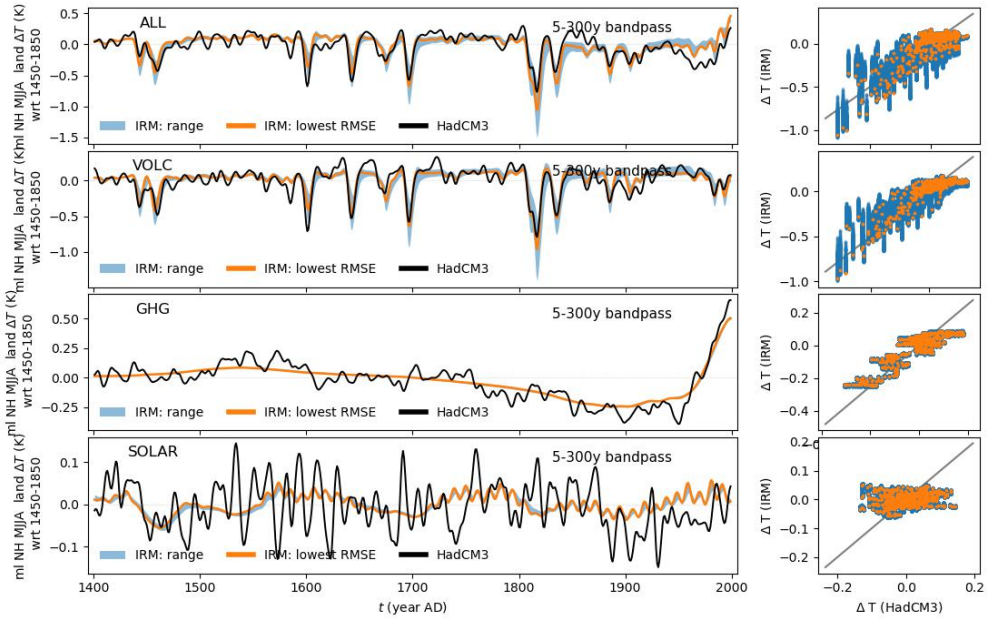

Figure S5: As previous but for tuning to midlatitudinal NH summer (MJJA).

index	Model name	30y chunks	170y chunks	runs: specification
1	ACCESS-CM2	16	2	r1i1p1f1 gn
2	ACCESS-ESM1-5	30	5	r1i1p1f1 gn
3	AWI-CM-1-1-MR	16	2	r1i1p1f1 gn
4	AWI-ESM-1-1-LR	3	0	r1i1p1f1 gn
5	BCC-CSM2-MR	20	3	r1i1p1f1 gn
6	BCC-ESM1	15	2	r1i1p1f1 gn
7	CAMS-CSM1-0	16	2	r1i1p1f1 gn
8	CESM2	40	7	r1i1p1f1 gn
9	CESM2-FV2	16	2	r1i1p1f1 gn
10	CESM2-WACCM	16	2	r1i1p1f1 gn
11	CESM2-WACCM-FV2	16	2	r1i1p1f1 gn
12	CNRM-CM6-1	16	2	r1i1p1f2 gr
13	CNRM-CM6-1-HR	10	1	r1i1p1f2 gr
14	CNRM-ESM2-1	16	2	r1i1p1f2 gr
15	CanESM5	48	7	r1i1p1f1 gn, r1i1p2f1 gn
16	E3SM-1-0	16	2	r1i1p1f1 gr
17	E3SM-1-1	5	0	r1i1p1f1 gr
18	E3SM-1-1-ECA	5	0	r1i1p1f1 gr
19	FGOALS-f3-L	18	3	r1i1p1f1 gr
20	FGOALS-g3	23	4	r1i1p1f1 gn
21	FIO-ESM-2-0	19	3	r1i1p1f1 gn
22	GFDL-CM4	16	2	r1i1p1f1 gr1
23	GFDL-ESM4	16	2	r1i1p1f1 gr1
24	GISS-E2-1-G	55	7	r101i1p1f1 gn, r102i1p1f1 gn, r1i1p1f1 gn, r1i1p1f2 gn, r1i1p1f3 gn, r2i1p1f1 gn
25	GISS-E2-1-G-CC	5	0	r1i1p1f1 gn
26	GISS-E2-1-H	13	2	r1i1p1f1 gn
27	GISS-E2-2-G	5	0	r1i1p1f1 gn
28	HadGEM3-GC31-LL	16	2	r1i1p1f1 gn
29	HadGEM3-GC31-MM	16	2	r1i1p1f1 gn
30	IITM-ESM	6	1	r1i1p1f1 gn
31	INM-CM4-8	17	3	r1i1p1f1 gr1
32	INM-CM5-0	40	7	r1i1p1f1 gr1
33	IPSL-CM6A-LR	74	12	r1i1p1f1 gr, r1i2p1f1 gr
34	MCM-UA-1-0	16	2	r1i1p1f1 gn
35	MIROC-ES2L	16	2	r1i1p1f2 gn
36	MIROC6	26	4	r1i1p1f1 gn
37	MPI-ESM-1-2-HAM	26	4	r1i1p1f1 gn
38	MPI-ESM1-2-HR	16	2	r1i1p1f1 gn
39	MPI-ESM1-2-LR	33	5	r1i1p1f1 gn
40	MRI-ESM2-0	23	4	r1i1p1f1 gn
41	NESM3	16	2	r1i1p1f1 gn
42	NorCPM1	48	6	r1i1p1f1 gn, r2i1p1f1 gn, r3i1p1f1 gn
43	NorESM1-F	6	1	r1i1p1f1 gn
44	NorESM2-LM	16	2	r1i1p1f1 gn
45	NorESM2-MM	16	2	r1i1p1f1 gn
46	SAM0-UNICON	23	4	r1i1p1f1 gn
47	TaiESM1	16	2	r1i1p1f1 gn
48	UKESM1-0-LL	62	11	r1i1p1f2 gn

Table S1: CMIP6 control runs (Eyring et al., 2016)

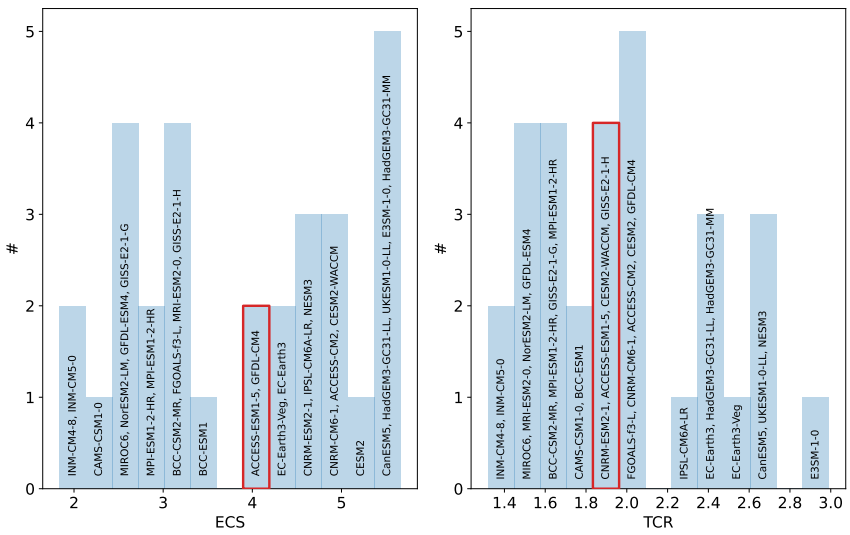

Figure S6: ECS and TCR values of the 30 CMIP6 models (Nijsse et al., 2020). Red shading indicates the median value.

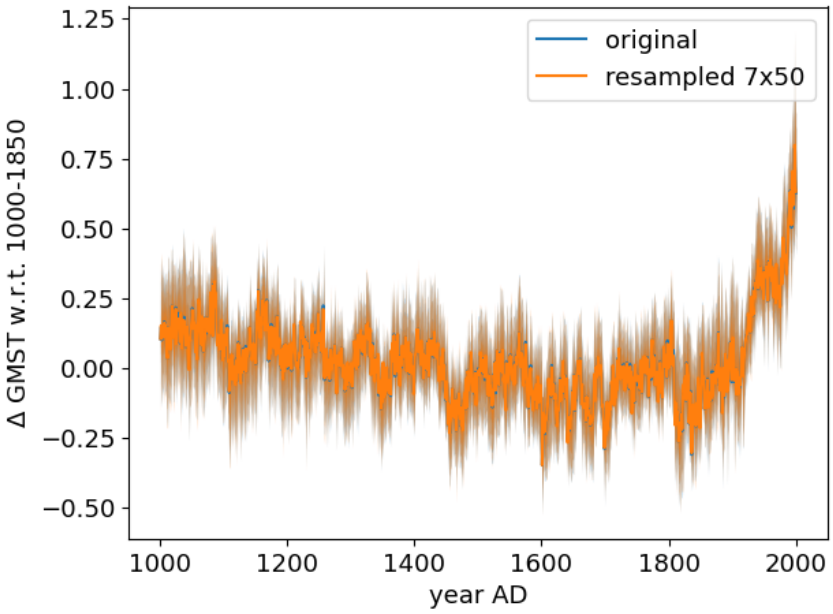

Figure S7: Subsampling of 7x50 members of the PAGES2k ensemble versus the full ensemble (7x1000 members)

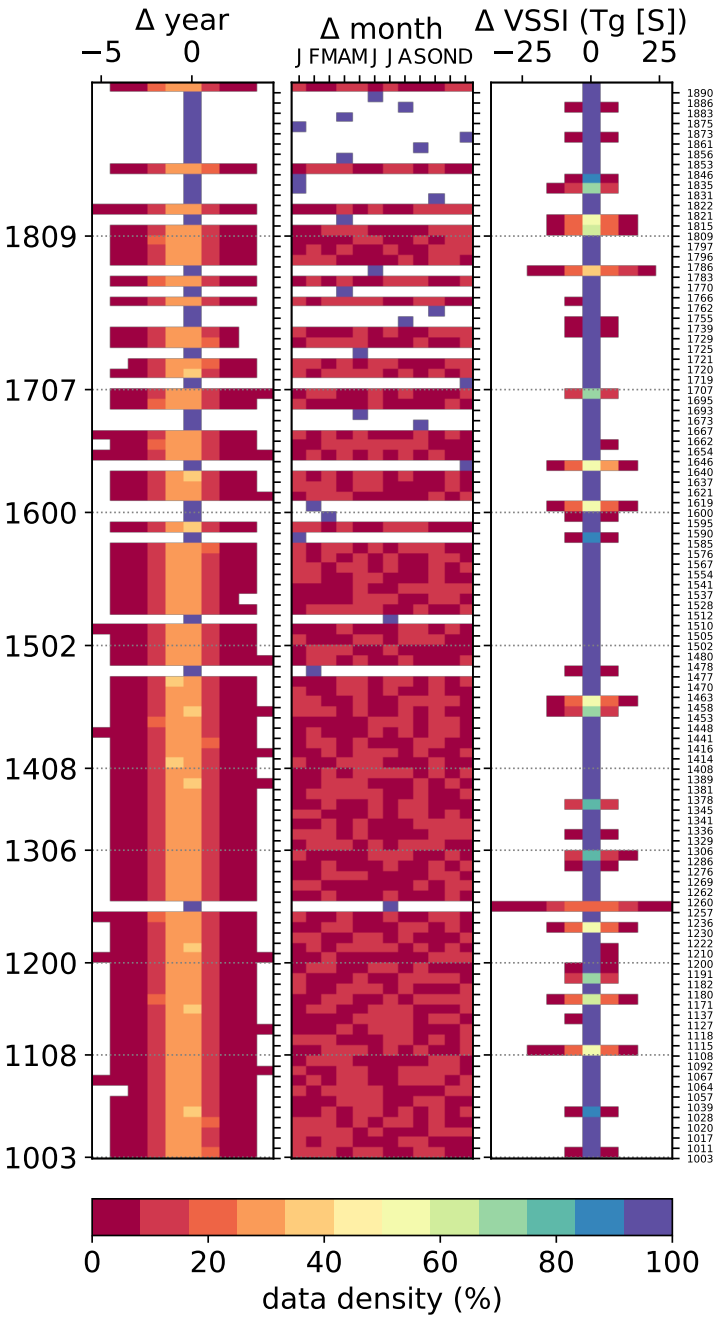

Figure S8: Overview of the volcanic forcing ensemble. Left: year of eruption relative to eVolv2k eruption year (eVolv2k eruption year shown on axis label of right panel). Middle: eruption month. Right: volcanic stratospheric sulfate injection (VSSI) relative to eVolv2k. Colour represents the data density. Blue single dots in left and middle panel are dated eruptions. Note that the time axis is not evenly spaced in time but by eruption years (see labels on right panel).

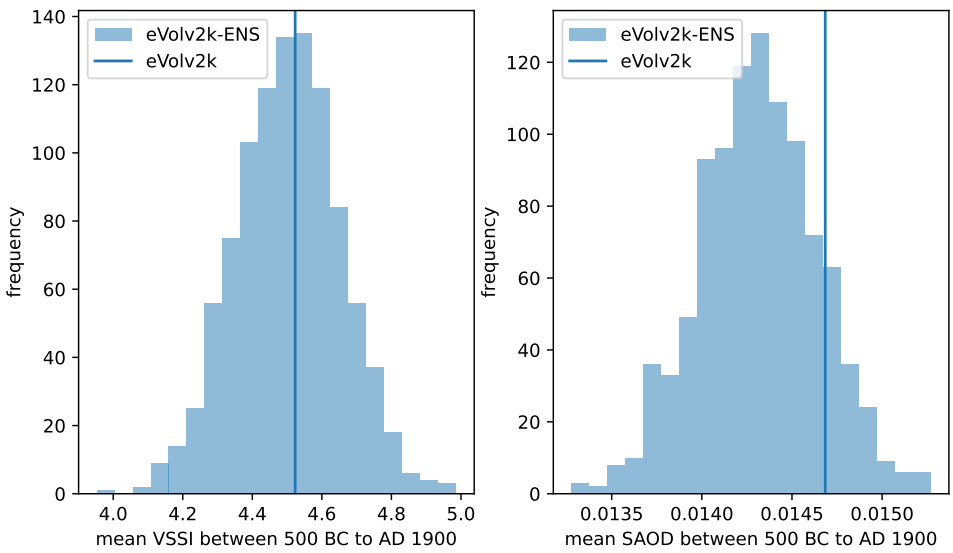

Figure S9: Left: mean VSSI of all eruptions between 500 BC and AD 1900 for eVolv2k and the distribution across eVolv2k-ENS. Right: as left panel but for mean SAOD.

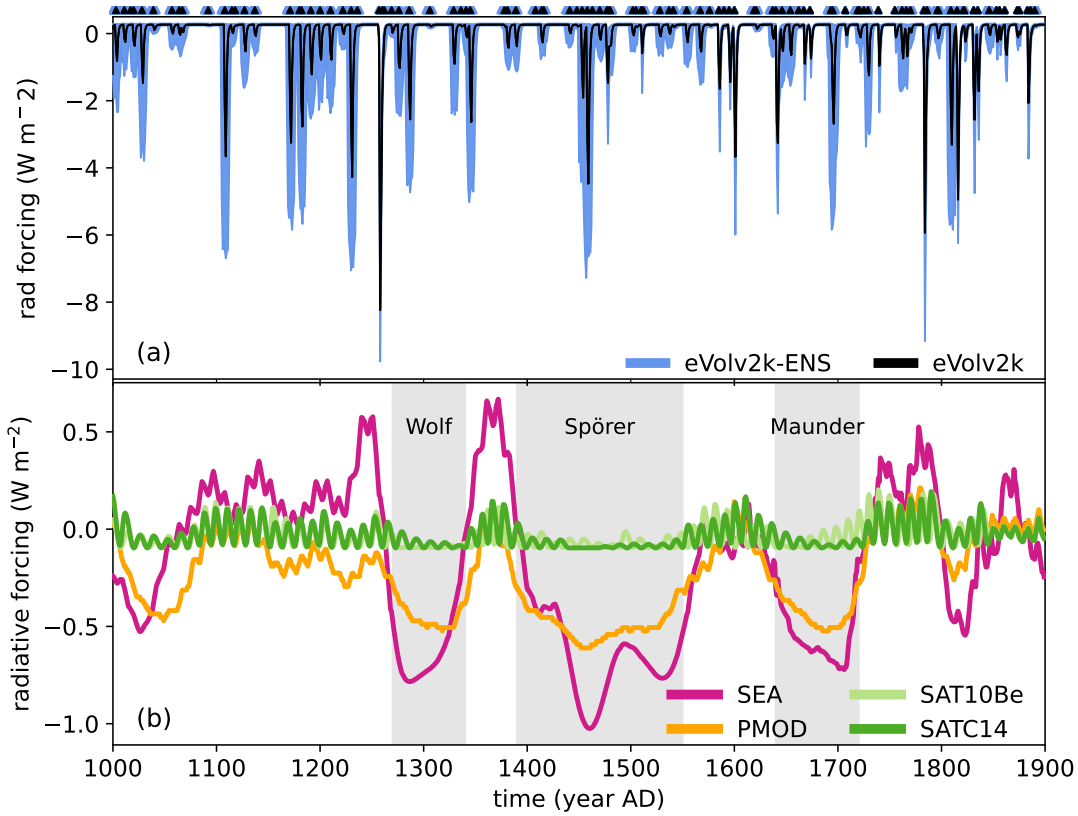

Figure S10: As Fig. 1 but with (a) showing NH radiative forcing.

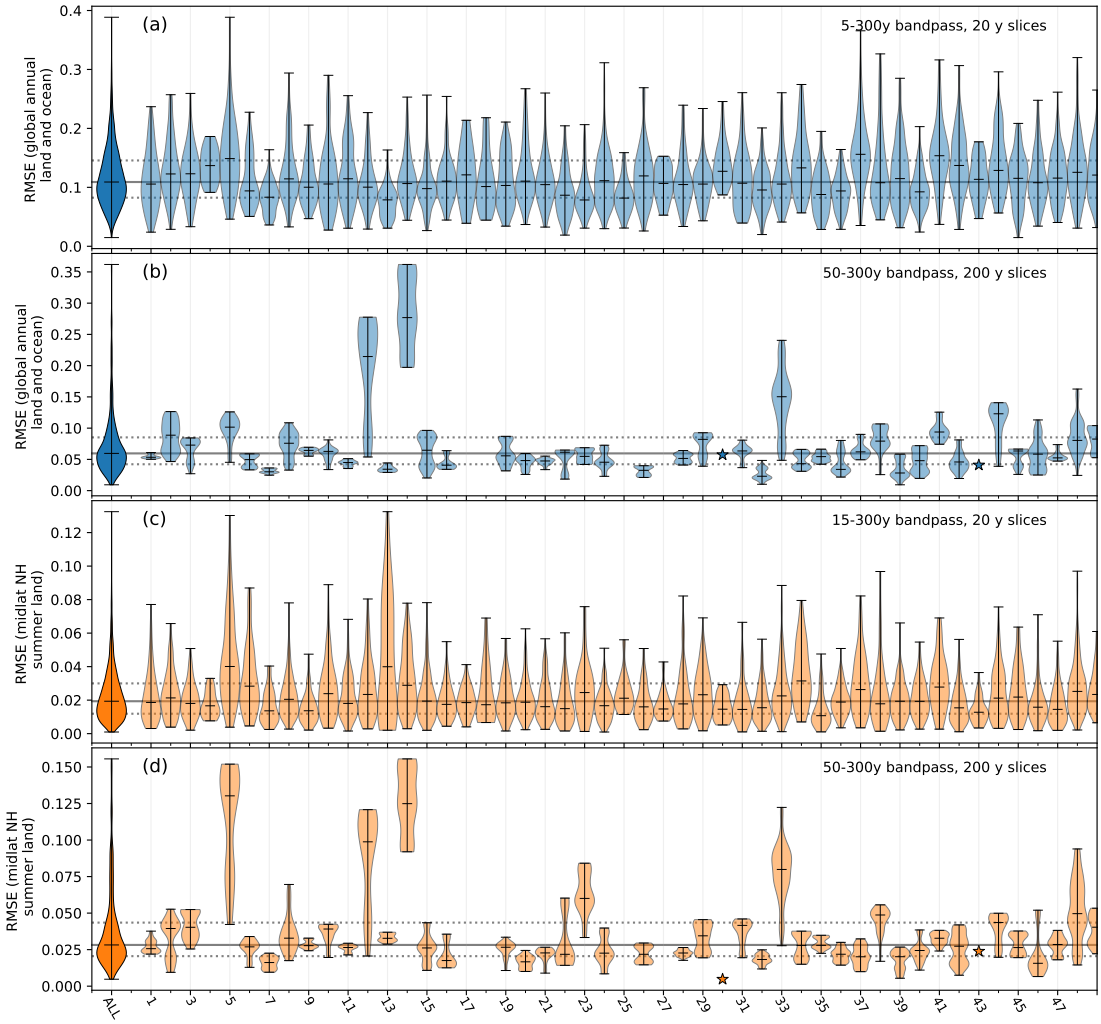

Figure S11: Variability of the individual CMIP6 control runs aggregated by model (see table S1 to identify the model names), and the whole CMIP6 population (ALL). (a), (b) non-overlapping 20 year slices (a) and 200 year slices (b) of midlatitudinal NH summer land temperature. (c) and (d) as (a) and (b) but for global annual data. The dashed horizontal line indicates the upper and lower quartile of the whole population. High variability models identified in (c) and (d) coincide with the ones identified by Parsons et al. (2020).

2 Solar uncertainty

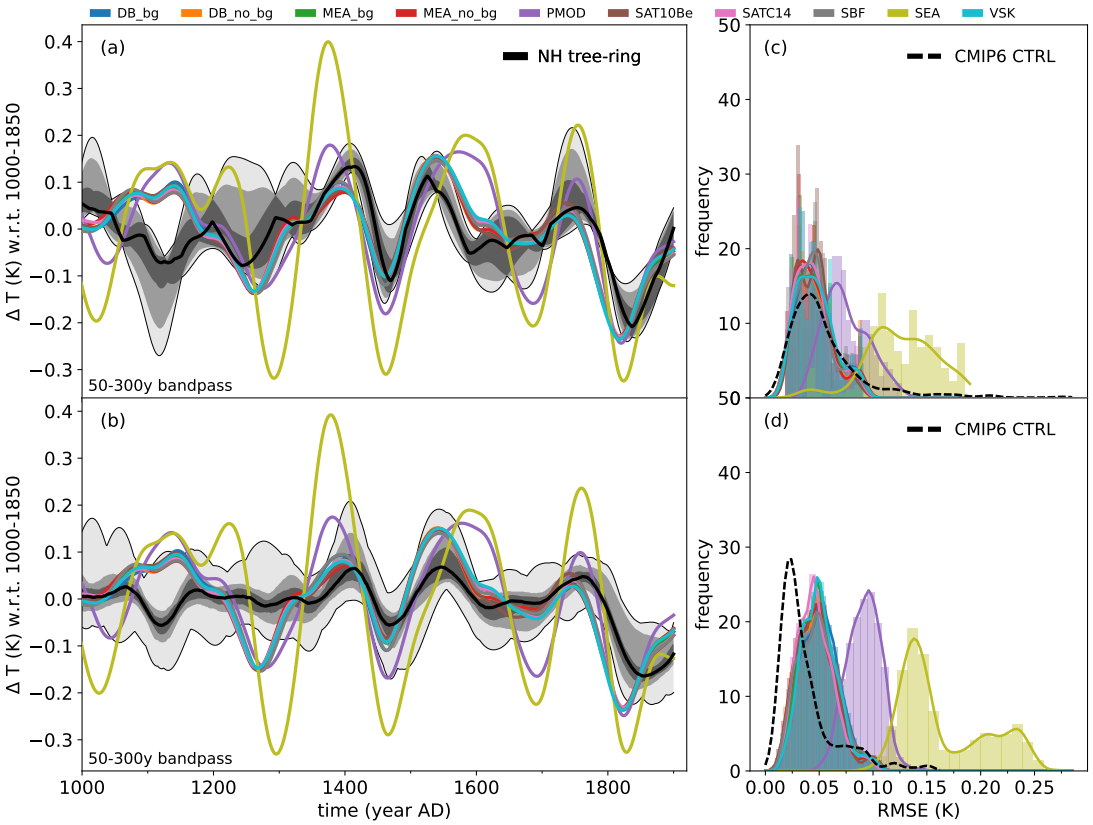

Figure S12: As Fig. 3 but for all solar forcings.

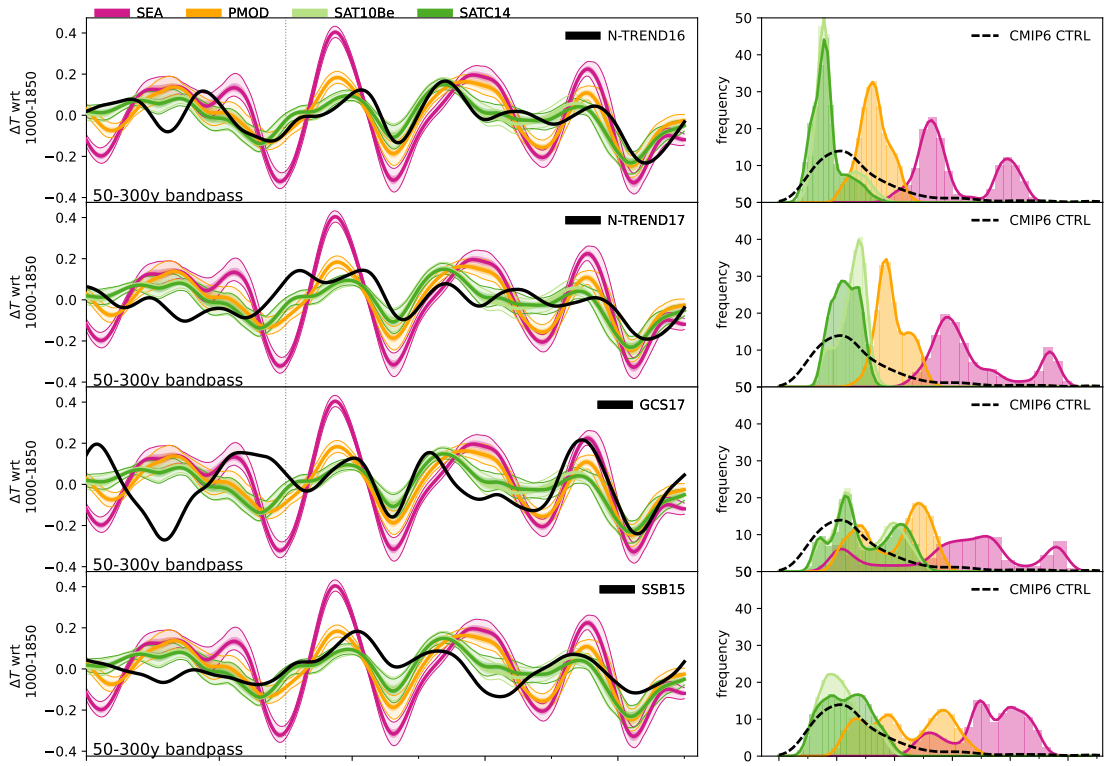

Figure S13: As Fig. 3 but for the single NH reconstructions. Top to bottom: N-TREND16 (Wilson et al., 2016), N-TREND17 (Anchukaitis et al., 2017), GCS17 (Guillet et al., 2017) and SSB15 (Schneider et al., 2015).

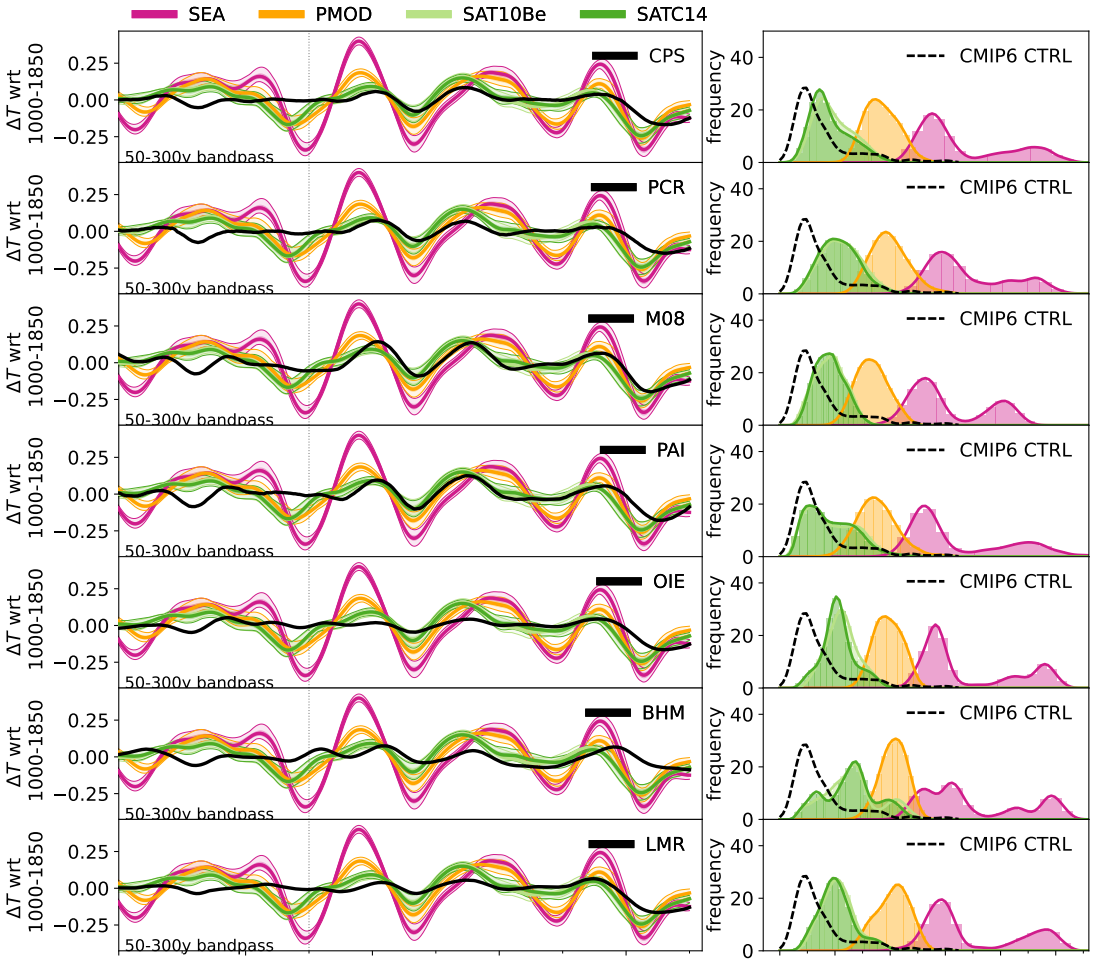

Figure S14: As Fig. 3 but for the single PAGES 2k median reconstructions.

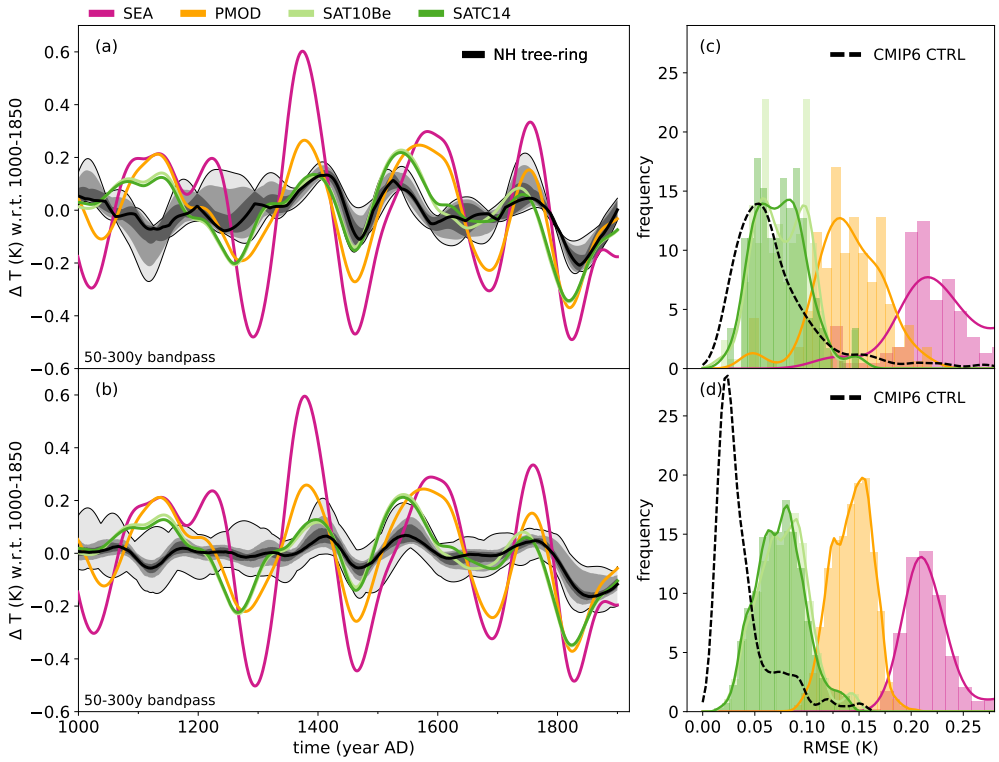

Figure S15: As Fig. 3 but for high climate sensitivity (ECS=5.38, TCR=2.99 as in E3SM-1-0).

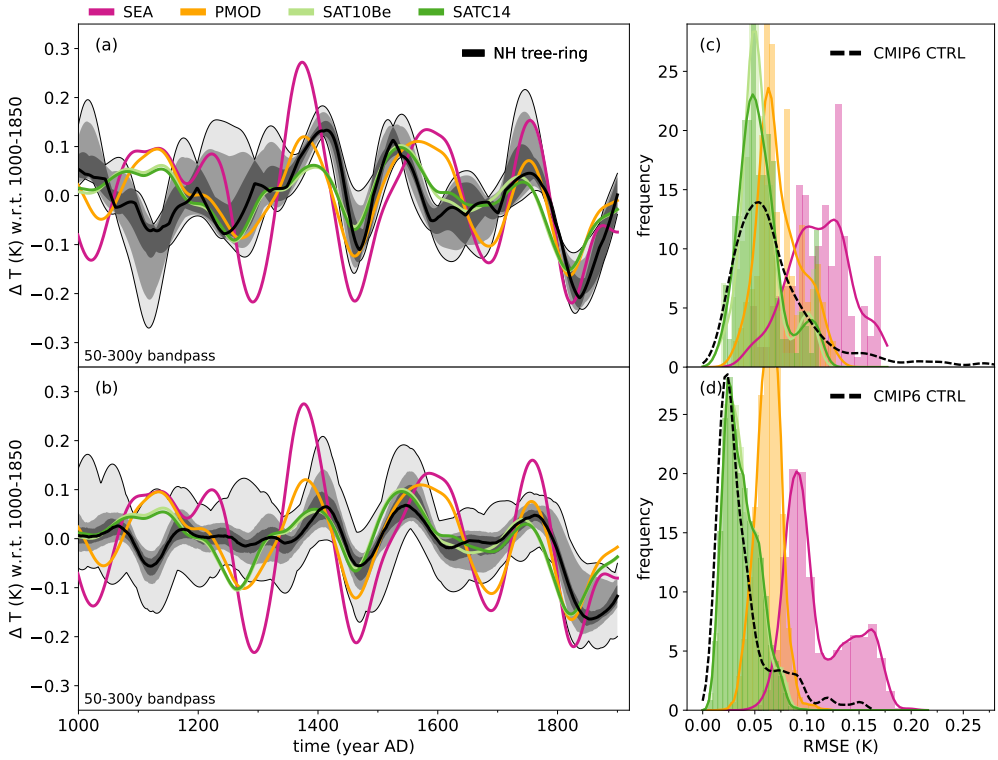

Figure S16: As Fig. 3 but for low climate sensitivity (ECS=1.84, TCR=1.32 as in INM-CM4-8).

3 Volcanic uncertainty

event	eVolv2k	eVolv2k–ENS lower	eVolv2k–ENS upper	eVolv2k–ENS best fit of N-TREND16	N-TREND17	GCS17	SSB15
	VSSI (Tg)						
1345	15.1	6.4 (42 %)	24.1 (159 %)	6.5 (42 %)	6.7 (44 %)	6.4 (42 %)	6.4 (42 %)
1453	10.0	0.0 (0 %)	19.5 (195 %)	12.6 (126 %)	12.5 (125 %)	17.2 (172 %)	12.5 (125 %)
1458	33.0	16.7 (50 %)	48.1 (145 %)	22.6 (68 %)	16.7 (51 %)	16.7 (51 %)	20.6 (62 %)
1600	18.9	6.2 (32 %)	34.1 (179 %)	11.2 (59 %)	8.5 (45 %)	11.2 (59 %)	6.6 (35 %)
1640	18.7	3.9 (20 %)	31.3 (167 %)	10.8 (58 %)	8.2 (44 %)	9.5 (51 %)	9.5 (51 %)
1695	15.7	6.4 (40 %)	25.4 (161 %)	13.9 (89 %)	9.8 (62 %)	16.9 (108 %)	13.2 (84 %)
1783	20.8	0.0 (0 %)	43.9 (210 %)	6.4 (31 %)	4.5 (22 %)	9.6 (46 %)	6.4 (31 %)
1809	19.3	6.9 (35 %)	30.8 (159 %)	9.5 (49 %)	9.5 (49 %)	20.3 (105 %)	6.9 (36 %)
1815	28.1	15.4 (54 %)	41.7 (148 %)	22.6 (80 %)	22.6 (80 %)	31.9 (114 %)	22.0 (78 %)
1831	13.0	2.3 (17 %)	22.0 (169 %)	2.3 (18 %)	4.9 (38 %)	9.2 (71 %)	7.1 (55 %)
1835	9.5	1.5 (15 %)	16.7 (176 %)	10.6 (112 %)	10.6 (112 %)	14.8 (156 %)	7.1 (75 %)
	eruption year						
1345	1345	1341 (−4)	1348 (+3)	1345 (±0)	1345 (±0)	1344 (−1)	1344 (−1)
1453	1453	1449 (−4)	1457 (+4)	1452 (−1)	1451 (−2)	1452 (−1)	1451 (−2)
1458	1458	1454 (−4)	1461 (+3)	1461 (+3)	1457 (−1)	1457 (−1)	1459 (+1)
1695	1695	1691 (−4)	1699 (+4)	1698 (+3)	1697 (+2)	1696 (+1)	1696 (+1)
1809	1809	1805 (−4)	1812 (+3)	1809 (±0)	1809 (±0)	1810 (+1)	1807 (−2)
	eruption month						
1345	Jan	Jan	Dec	Aug	Sep	Mar	Mar
1453	Jan	Jan	Dec	Aug	April	Sep	Mar
1458	Jan	Jan	Dec	June	Nov	Nov	Mar
1695	Jan	Jan	Dec	Jan	Jan	April	Mar
1809	Jan	Jan	Dec	Mar	Mar	July	Nov

Table S2: Eruption specific parameters (VSSI, eruption year, eruption month) for eVolv2k and for the associated best fit eVolv2k–ENS member favoured by the different NH tree-ring reconstructions. Eruption year and month are only shown for the undated eruptions. The relative values compared to eVolv2k are shown in brackets: for VSSI the ratio, for eruption year the difference.

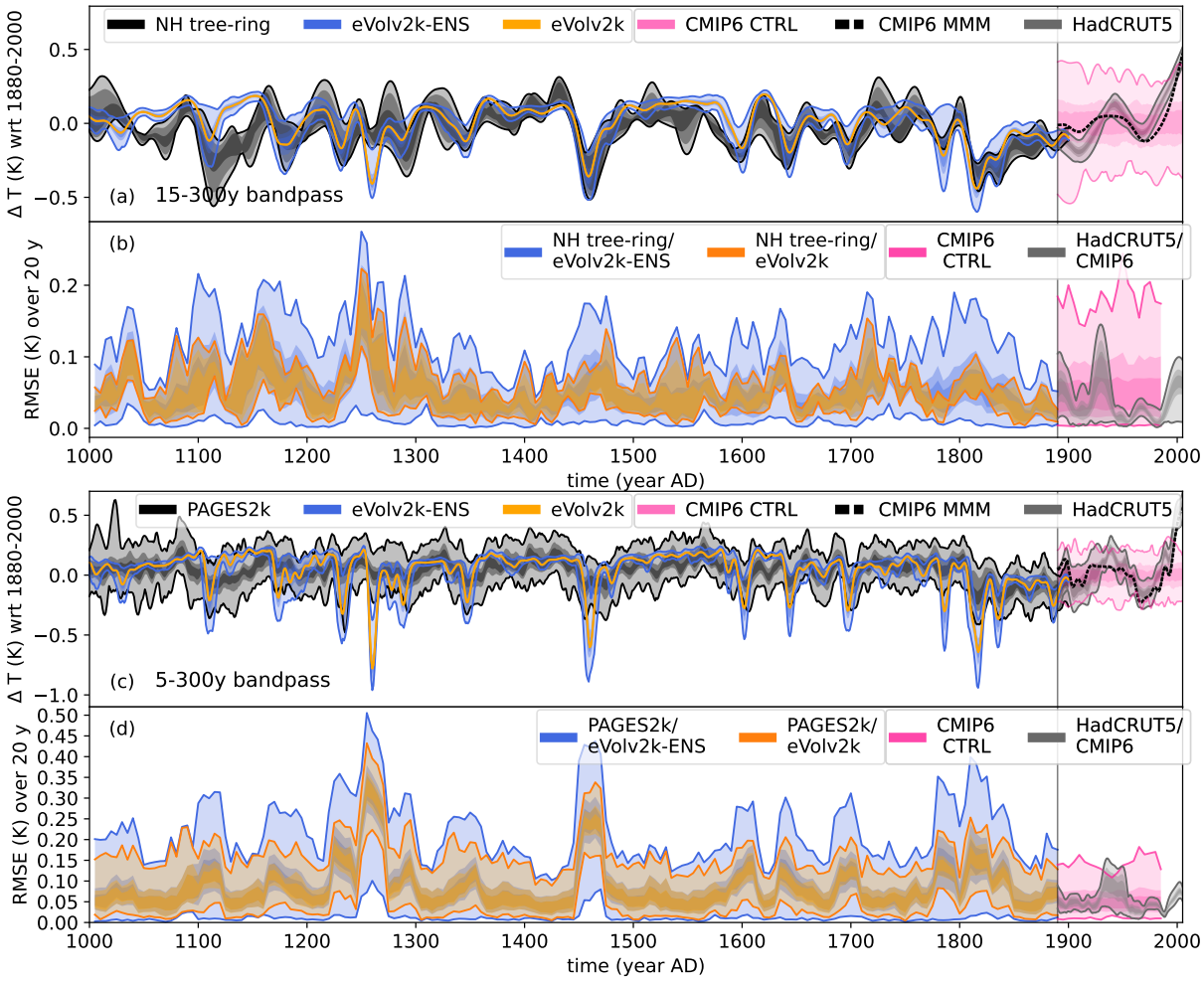

Figure S17: As Fig. 4 but with inverted bandpass filters for NH reconstructions and PAGES 2k.

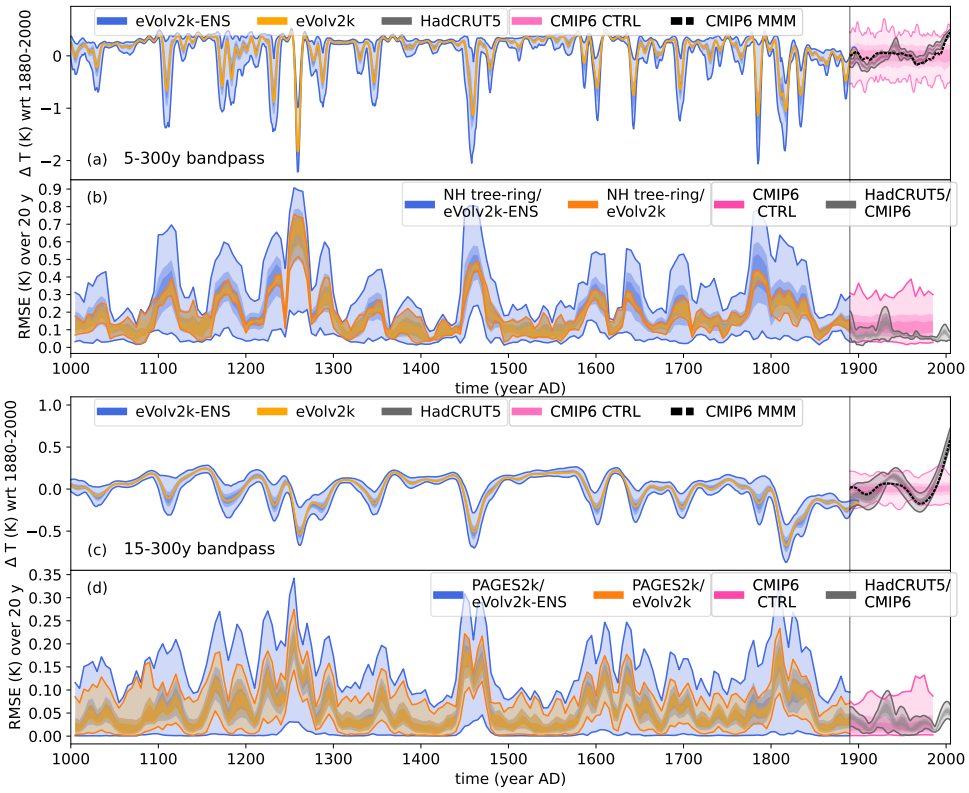

Figure S18: As Fig. 4 but for high climate sensitivity (ECS=5.38, TCR=2.99 as in E3SM-1-0).

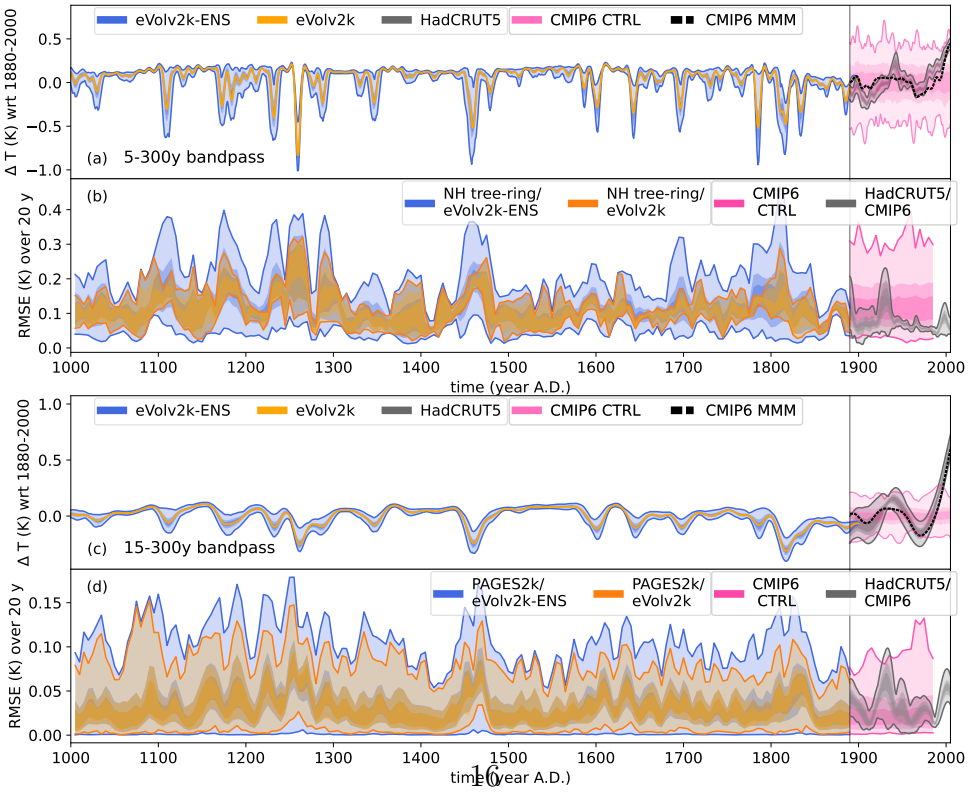

Figure S19: As Fig. 4 but for low climate sensitivity (ECS=1.84, TCR=1.32 as in INM-CM4-8).

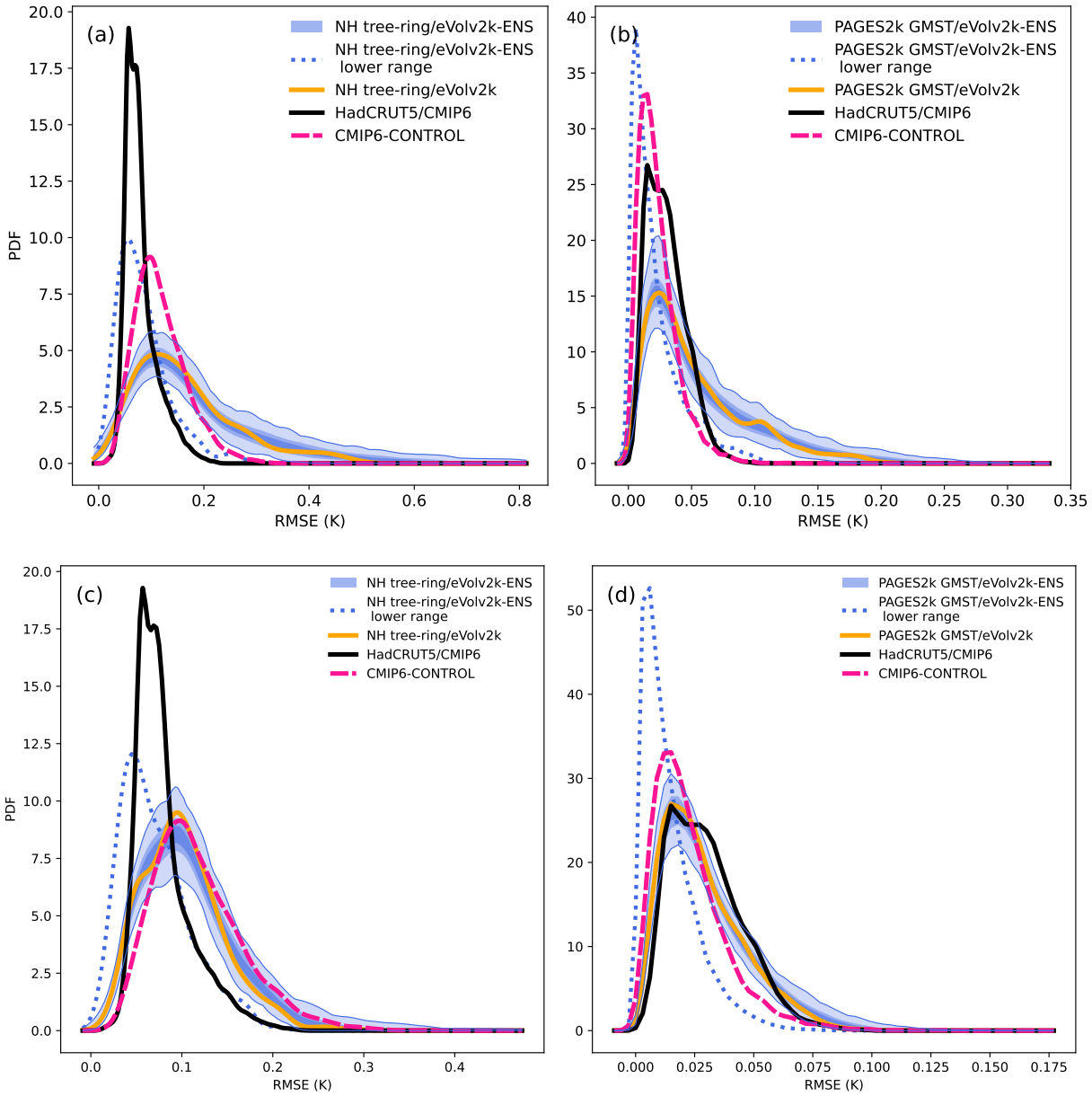

Figure S20: As Fig. 5 but for (a), (b) high climate sensitivity (ECS=5.38, TCR=2.99 as in E3SM-1-0) and for (c), (d) low climate sensitivity (bottom, ECS=1.84, TCR=1.32 as in INM-CM4-8).

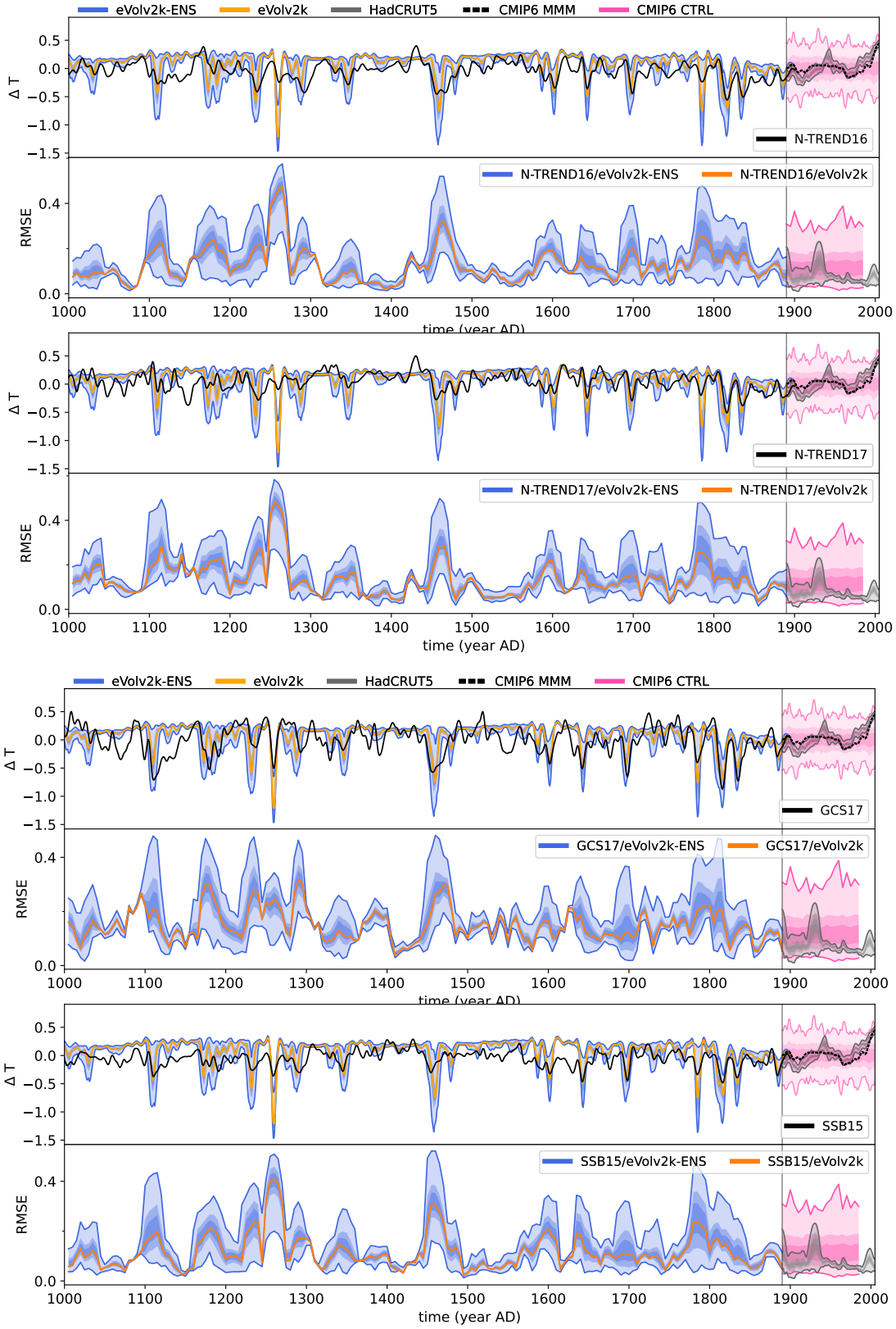

Figure S21: As Fig. 4 but for single NH reconstructions. Top to bottom: N-TREND16 (Wilson et al., 2016), N-TREND17 (Anchukaitis et al., 2017), GCS17 (Guillet et al., 2017) and SSB15 (Schneider et al., 2015)

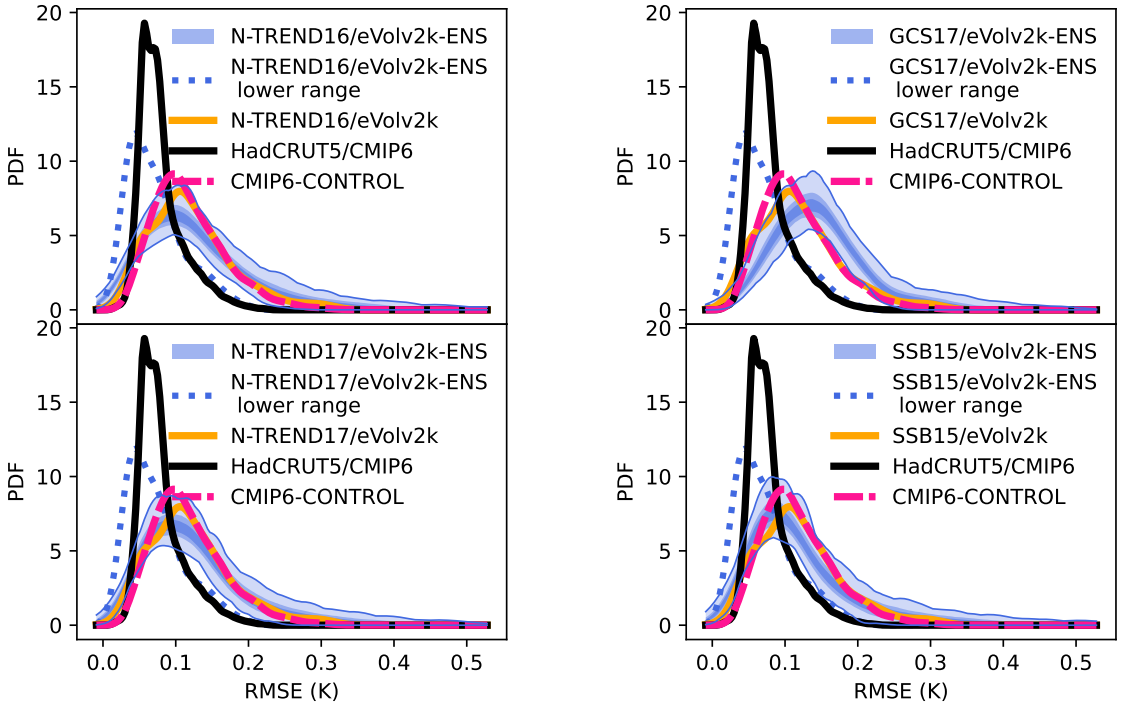

Figure S22: As Fig. 5 but for single NH reconstructions. Left top to bottom: N-TREND16 (Wilson et al., 2016), N-TREND17 (Anchukaitis et al., 2017), Right top to bottom: GCS17 (Guillet et al., 2017) and SSB15 (Schneider et al., 2015).

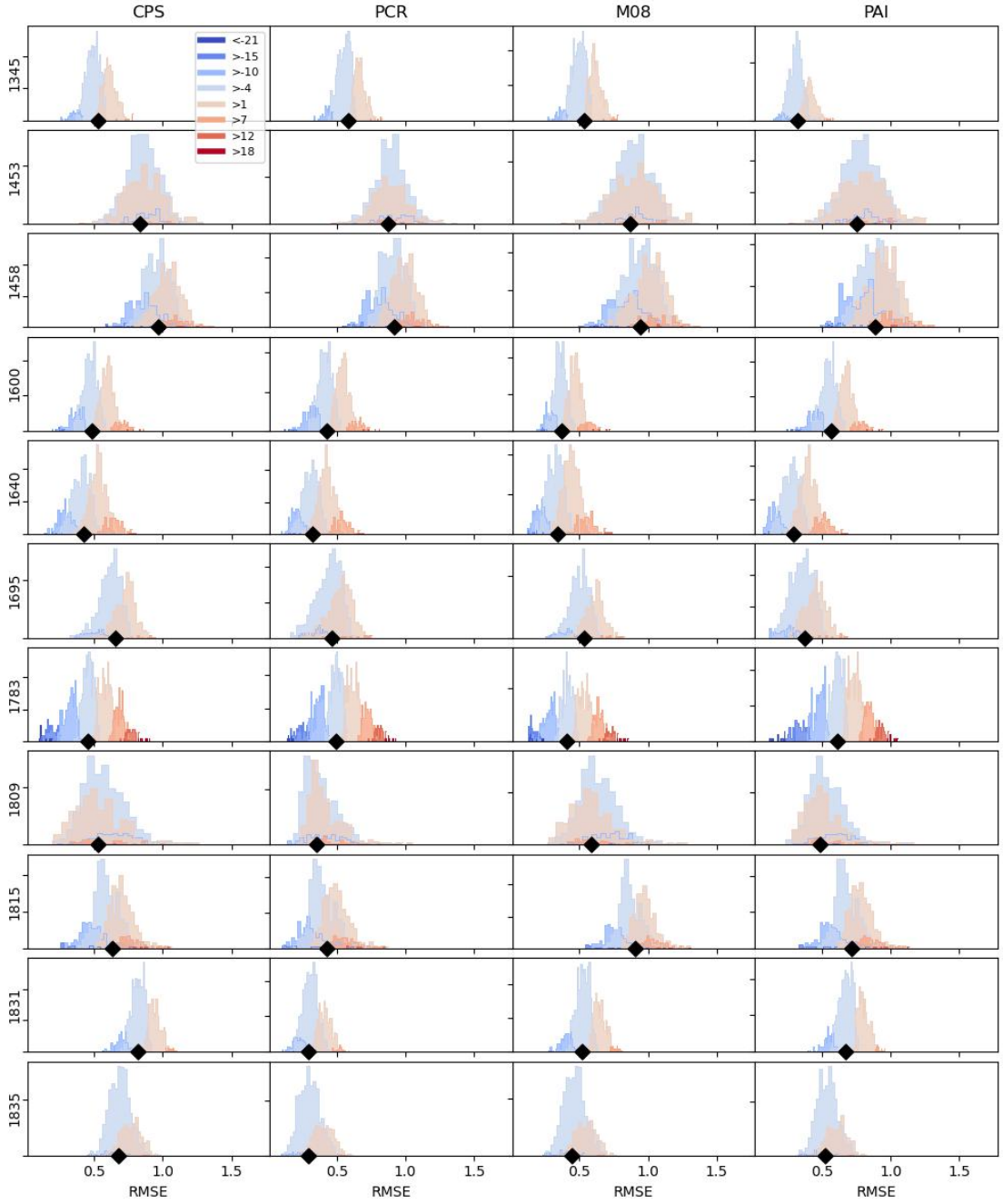

Figure S23: Distribution of average residual between NH reconstructions and each member of eVolv2k-ENS, starting in eruption year to 15 years after. In all panels, the data is colour coded depending on the eruption difference in VSSI compared to eVolv2k (see legend in first panel). Black diamond on x-axis shows the RMSE associated with eVolv2k.

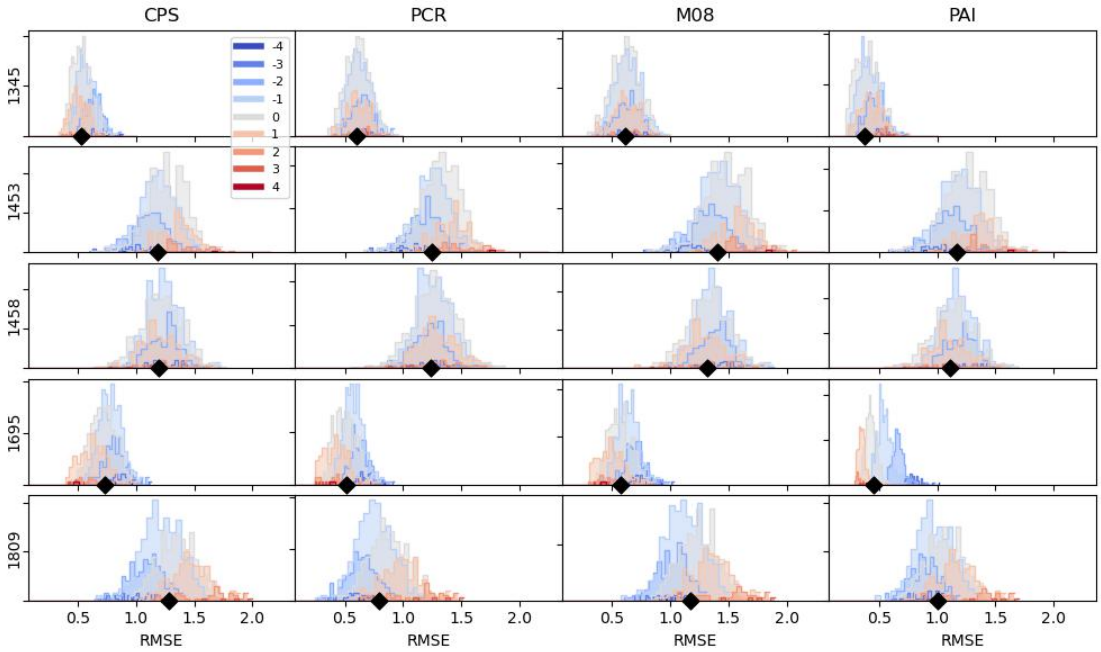

Figure S24: As Fig. S23, but showing the difference in eruption year for the undated eruptions only.

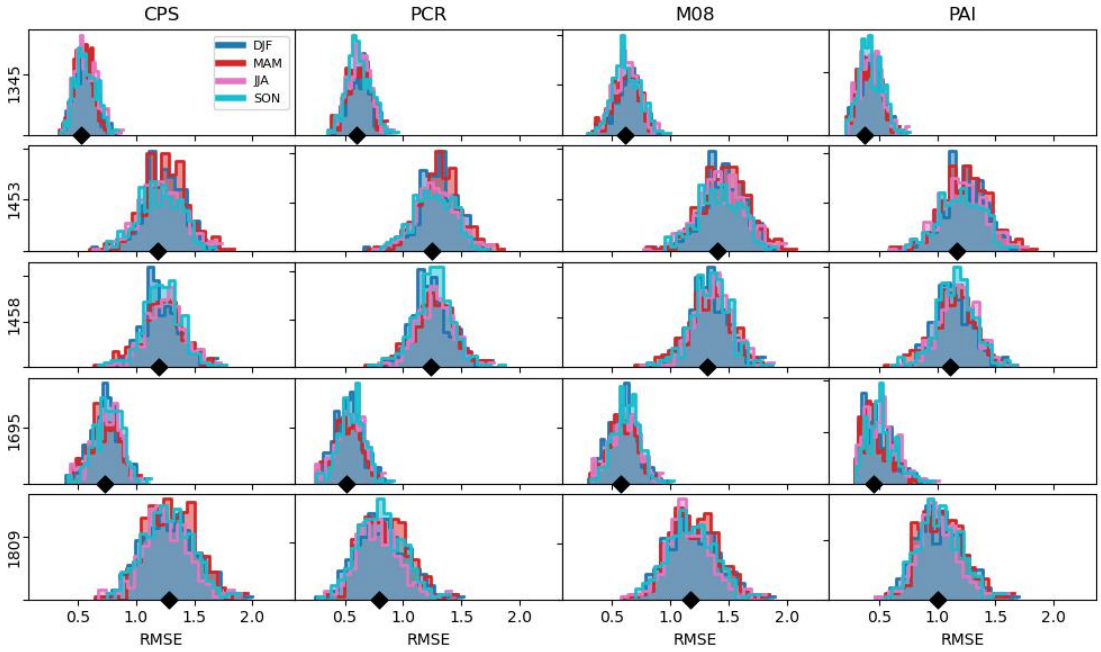

Figure S25: As Fig. S24, but showing the eruption season. In eVolv2k all eruptions are assigned to happen in January.

References

Anchukaitis, Kevin J. et al. (May 2017). "Last millennium Northern Hemisphere summer temperatures from tree rings: Part II, spatially resolved reconstructions". In: *Quaternary Science Reviews* 163, pp. 1–22. DOI: 10.1016/j.quascirev.2017.02.020.

Eyring, Veronika et al. (May 2016). "Overview of the Coupled Model Intercomparison Project Phase 6 (CMIP6) experimental design and organization". In: *Geoscientific Model Development* 9.5, pp. 1937–1958. DOI: 10.5194/gmd-9-1937-2016.

Guillet, Sébastien et al. (Jan. 2017). "Climate response to the Samalas volcanic eruption in 1257 revealed by proxy records". In: *Nature Geoscience* 10.2, pp. 123–128. DOI: 10.1038/ngeo2875.

Nijsse, Femke J. M. M., Peter M. Cox, and Mark S. Williamson (Aug. 2020). "Emergent constraints on transient climate response (TCR) and equilibrium climate sensitivity (ECS) from historical warming in CMIP5 and CMIP6 models". In: *Earth System Dynamics* 11.3, pp. 737–750. DOI: 10.5194/esd-11-737-2020.

Parsons, Luke A. et al. (Apr. 2020). "Magnitudes and Spatial Patterns of Interdecadal Temperature Variability in CMIP6". In: *Geophysical Research Letters* 47.7. DOI: 10.1029/2019gl086588.

Schneider, Lea et al. (June 2015). "Revising midlatitude summer temperatures back to A.D. 600 based on a wood density network". In: *Geophysical Research Letters* 42.11, pp. 4556–4562. DOI: 10.1002/2015gl063956.

Wilson, Rob et al. (Feb. 2016). "Last millennium northern hemisphere summer temperatures from tree rings: Part I: The long term context". In: *Quaternary Science Reviews* 134, pp. 1–18. DOI: 10.1016/j.quascirev.2015.12.005.